Variable-speed operation and pressure pulsations in a Francis turbine and a pump-turbine

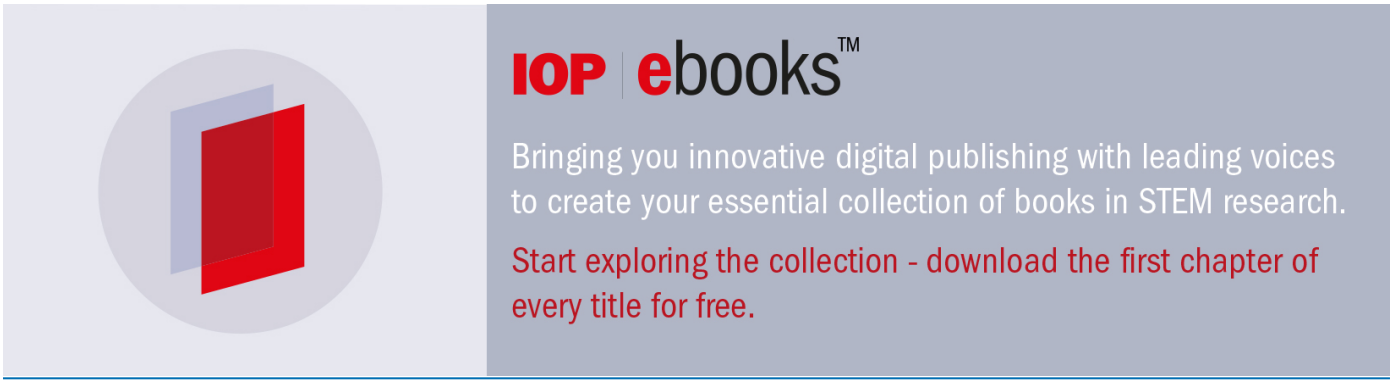

Variable-speed operation and pressure pulsations in a Francis turbine and a pump-turbine

I Iliev[1*], C Trivedi[1], E Agnalt[1] and O G Dahlhaug[1]

[1]Waterpower Laboratory, Department of Energy and Process Engineering, Norwegian University of Science and Technology, Alfred Getz Vei 4, Trondheim, Norway

E-mail: igor.iliev@ntnu.no

Abstract. The paper presents result from model measurements of the efficiency and pressure pulsation intensities for two low-specific-speed hydraulic turbines operated at variable speed, namely, one splitter-bladed Francis turbine marked with "F99" and one reversible pump-turbine marked with "RPT" and operated in a turbine mode. Both turbines have similar specific speeds, i.e. $n_{QH}^{(F99)} = 21.88$ and $n_{QH}^{(RPT)} = 27.26$, and for their best efficiency points, both have similar guide-vane opening angles but different operating parameters (i.e., speed factor and discharge factor). Pressure pulsation measurements were conducted for a wide operating range and at specific locations in the (1) vaneless space and (2) draft tube. Histogram method was used to obtain the peak-to-peak amplitudes of the fluctuating pressure for all operating points used to construct the performance hill-charts of the turbines. To the best of the authors' knowledge, very little or no effort has been made so far to explore the amplitudes of pressure pulsations in the turbine when operated at rotational speeds specifically optimized for maximization of the hydraulic efficiency. Results show that operation of Francis turbines at optimized rotational speeds can increase the hydraulic efficiency of the turbine, while decreasing or maintaining the same pressure pulsation amplitudes in the entire operational range. Also, it was found that the level of efficiency gain and reduction of the pressure pulsations is greatly dependent on the hydraulic design of the turbine and should be investigated individually for each case.

1. Introduction

Operation of Francis turbines away from the design conditions will result in reduction of the hydraulic efficiency, accompanied by unstable and pulsating flow structures being developed in the turbine passages. Consequently, pressure pulsations are produced which can lead to an unstable and harmful operation of the machine [1, 2]. On the other hand, due to the increased usage of intermittent energy sources like solar and wind, hydropower is also expected to provide ancillary services for grid stabilization and production/consumption balance. Today's demands for additional flexibility of hydropower plants have considerably increased the off-design operation time of Francis turbines that can cause structural failures and material cracks [3-6].

In a conventional turbine design, the runner is rotating at a constant (synchronous) speed due to the direct connection of the generator to the grid [7]. This type of operation will result in a larger movement of the operating point away from the best efficiency point (BEP) in the hill-chart area of the turbine, eventually leading to operational zones with a higher dynamic load. A common source for deterministic pressure pulsations are the Rotor-Stator Interaction (RSI) and the corkscrew vortex precession in the draft-tube, while stochastic pressure pulsations originate from boundary layer effects and secondary flows in the turbine passages. Experimental and numerical studies on different types of

Francis turbines have showed that both deterministic and stochastic dynamic loads are dependent on the operating point of the turbine [1]. In addition, depending on the location where measurements are taken, normalized amplitudes for characteristic pressure pulsations will have different values.

To reduce the amplitudes of pressure pulsations, experiments with variable-speed operation of the turbine runner had been carried out. Variable-speed operation offers the possibility to limit the movement of the operating point in the hill chart area, hence avoiding harmful zones while increasing the off-design efficiency of the turbine [8-11]. Using full-power converters or induction generators omits the need for synchronism between the production unit and the grid, thus allowing the speed to be freely adjusted according to the flow conditions and needs [12-14]. In order to achieve a safe variable-speed operation of Francis turbines, amplitudes of pressure pulsations for the entire operating range have to be identified and analyzed.

2. Experimental setup and instrumentation

The measurements were carried out at the Waterpower laboratory at the Norwegian University of Science and Technology (NTNU) in Trondheim, Norway. The Francis turbine test-rig can be operated in a closed or open loop configuration, depending on the purpose of the measurements and in compliance with the international standard for model tests [15]. In the present work, measurements were done in an open loop, providing easer control of the rig and faster stabilization of the new operating condition each time changes were made. Also, for the particular head of the models, the setting level in the open loop was sufficient to provide a cavitation-free conditions for the entire operating range of both runners. Therefore, the obtained results and analysis presented hereafter are strictly applicable for cavitation-free operation only, since the pressure fluctuations are highly dependent on the cavitation conditions [16].

Part of the test-rig between the high-pressure and low-pressure tanks is shown on figure 1, where the water was pumped from a basement sump into an attic tank (not shown) and further directed down to the high-pressure tank by its natural head. Then, the water passes through the Francis turbine test rig, into the low-pressure tank and back into the sump.

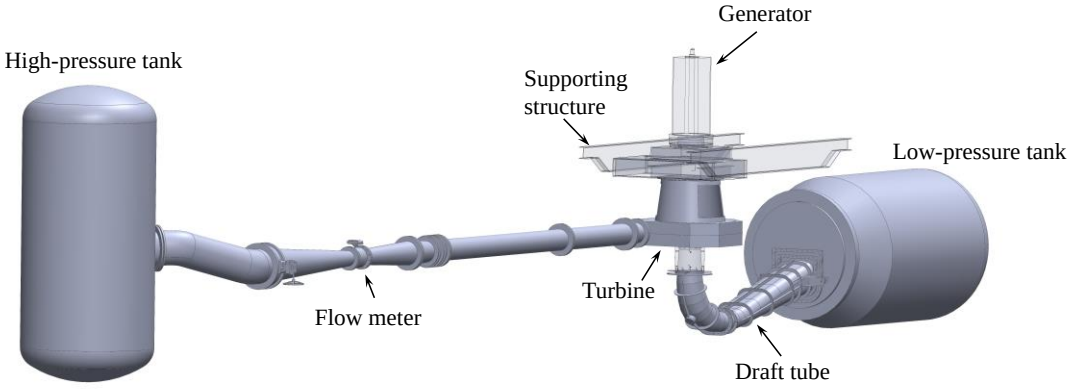

Figure 1. Section of the test rig at the Waterpower Laboratory at NTNU.

Two different turbine runners were tested at the same rig, namely, one splitter-bladed Francis turbine marked with “F99” and one reversible-pump turbine marked with “RPT” (see figure 2). Both runners originate from different research activities at the Waterpower laboratory, with the RPT runner specifically designed to fit in the distributor and draft tube configuration of the F99. Hence, they have equal inlet and outlet diameters and equal distance between the hub and shroud at the inlet of the runners (channel width). The F99 runner was designed as a reference runner to study RSI and Fluid-Structure Interactions (FSI) problems in high-head Francis turbines [17], while the RPT runner was designed to study the instable behavior at part-load for high head and low specific speed pump-turbines [18].

Steady-state measurements were done for more than 200 operating points for each turbine runner, and data was recorded for: (1) the global operating parameters of the turbine needed to construct the performance hill charts, and (2) the pressure pulsations in the draft-tube and the vaneless space between

the guide-vanes and the runner blades (see figure 3). Global parameters monitored are: generator torque, friction torque, differential pressure between the inlet and outlet sections of the turbine, atmospheric pressure, inlet pressure, outlet pressure, rotational speed, discharge and water temperature. The operating range of the global parameters for both turbine runners are given in table 1.

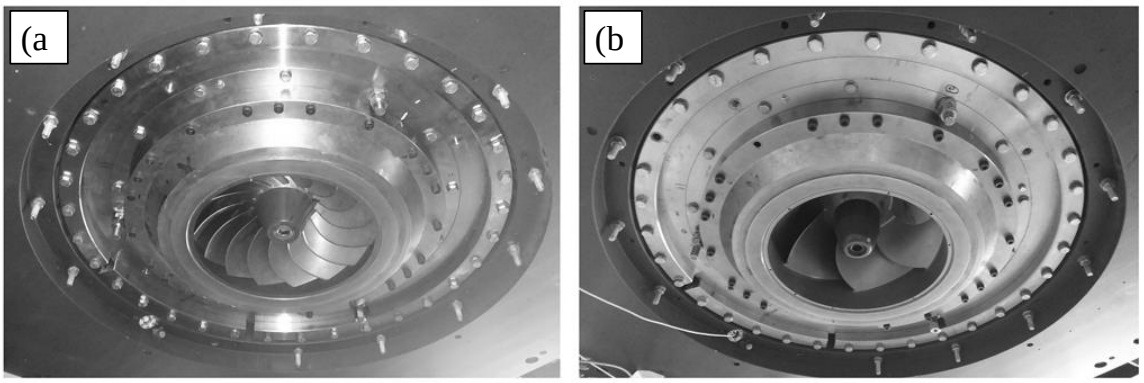

Figure 2. Outlet view of both runners during installation, before the draft-tube cone is being connected. a) Francis turbine F99 with 15 full-length blades and 15 splitter blades, b) Reversible pump-turbine RPT with 6 full-length blades.

Pressure pulsations between the guide vanes and in the vaneless space were recorded using six flush mounted TE XP5 and Kulite XTE active sensors marked with GV1 to GV6 (see figure 3) in the stream wise direction, transduced using Wheatstone bridge (National Instruments DAQ modules). In the draft tube cone, two measuring planes were defined, where two pressure sensors shifted by 180 degrees (opposite to each other) were installed at each plane, resulting in four sensors marked with DT1 to DT4. In the upper plane, closer to the runner, Kulite HKM sensors were used, whereas in the lower plane (downstream the upper plane), two flush mounted Kistler dynamic piezo-sensors were used connected to Kistler charge amplifiers for preconditioning of the signal. Data was acquired and recorded using NI LabVIEW program with a logging frequency of 10 kHz and recording time of 60 seconds. Oversampling was used to provide a wide alias-free bandwidth with the necessary frequency resolution in the signal, while 60 seconds was enough to capture all transients having lowest frequencies. Additional components for signal conditioning are also included in the measurement system, such as amplifiers, analog filters and analog-to-digital converters (ADC), used to provide the lowest possible noise interference and proper quality of the stored digital signal. Amplification was matched to the ADC range and the cutoff frequency of the analog filter was set to a value lower than half the sampling rate to avoid aliasing in the frequency spectrum.

Table 1. Operating range and BEP values for both turbine runners tested.

	F99		**RPT**	
Parameter	BEP	Range	BEP	Range
$H\ [m]$	12	/	12	/
$\alpha_{GV}\ [deg]$	9	4 – 14	10.8	4 – 14
$n\ [rpm]$	322	220 – 450	412	310 – 510
$Q\ [l/s]$	192	60 – 310	182	80 – 230
$n_{ED}\ [-]$	0.1725	0.12 – 0.24	0.221	0.17 – 0.27
$Q_{ED}\ [-]$	0.145	0.045 – 0.24	0.138	0.06 – 0.17
$\eta\ [\%]$	92.6	/	89.6	/
$n_{QH}\ [rpm\ m^{3/4}\ s^{-1/2}]$	21.88	/	27.26	/

Dead weight calibration of the pressure sensors was done having the sensors connected through the whole electrical chain and before mounting them on the rig. Calibration of the equipment used to

measure the overall performance of the turbine was done with compliance to the international standard [15], achieving the needed level of accuracy for model tests.

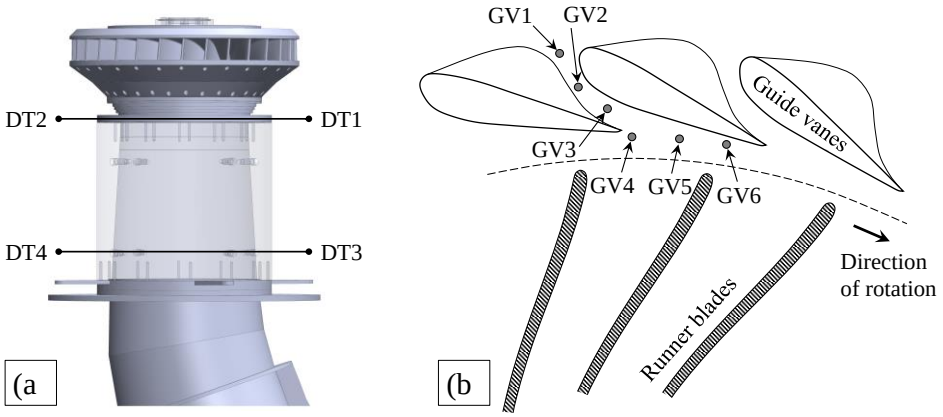

Figure 3. Locations of the pressure sensors in the: a) draft tube cone, b) guide vane and vaneless space.

Due to the correlation and similarities for the signals recorded with different sensors, analysis of the pressure pulsations is done only for GV5 in the vaneless space and DT1 and DT3 from both planes in the draft tube cone, with the rest not included in this paper.

3. Description of data analysis using the histogram method

Pressure pulsation intensities are quantified using the *histogram method* for the *peak-to-peak values* computed from the time series recorded at the investigated locations in the turbine [1, 15]. In its statistical definition, histogram method is a probability density curve of the sampled values where some percentage of the upper and lower part of the respective probability distribution is discarded. According to a footnote suggestion related to pressure fluctuations from the IEC 60193 standard, a middle part of 97% of the values should be retained with 1.5% discarded from both sides. The peak-to-peak value is then calculated as the difference between the *min* and *max* values on the remaining middle part of the histogram (see figure 4). In a rather detailed analysis, Dorfler et al. [1] have compared different methods for calculation of the double-amplitudes of the pressure fluctuations and found that a scatter exists between various definitions, especially when the recorded signal has stochastic content. However, despite the dependence of the peak-to-peak value on the chosen percentage, Dorfler et al. reported that a histogram method with 97% would produce the most unambiguous results for such analysis.

Figure 4 illustrates the method and the peak-to-peak values calculated for a single operating point of the F99 runner at guide vane opening of $\alpha_{GV} = 6\ [deg]$ and speed factor of $n_{ED} = 0.18\ [-]$ for the three investigated locations GV5, DT1 and DT3. The full length of the recorded signal was used, with the mean value being suppressed and the resulting signal being digitally filtered with a zero-phase low-pass filter with cutoff frequency set at 1 kHz. The deviation from the mean value is marked with Δp and normalized with the product of the specific energy E and the water density ρ. Signal length of 30 runner revolutions, corresponding to approximately 5.4 seconds, is shown on the diagrams on the left side of figure 4. The diagrams on the right side of the same figure show the histogram representations of the full length of the same signals. The area in the middle of the probability density curve, between the bold vertical lines defining the peak-to-peak range, represents the remaining 97% of the data after discarding the 3% least probable values. Calculated peak-to-peak values (the distance between the black tick lines in the diagrams on figure 4) shows good agreement with the actual pulsation intensities of the time series (see signal history on the left hand side). Outliers in the signal that happen rarely are correctly handled to have very low influence on the peak-to-peak value.

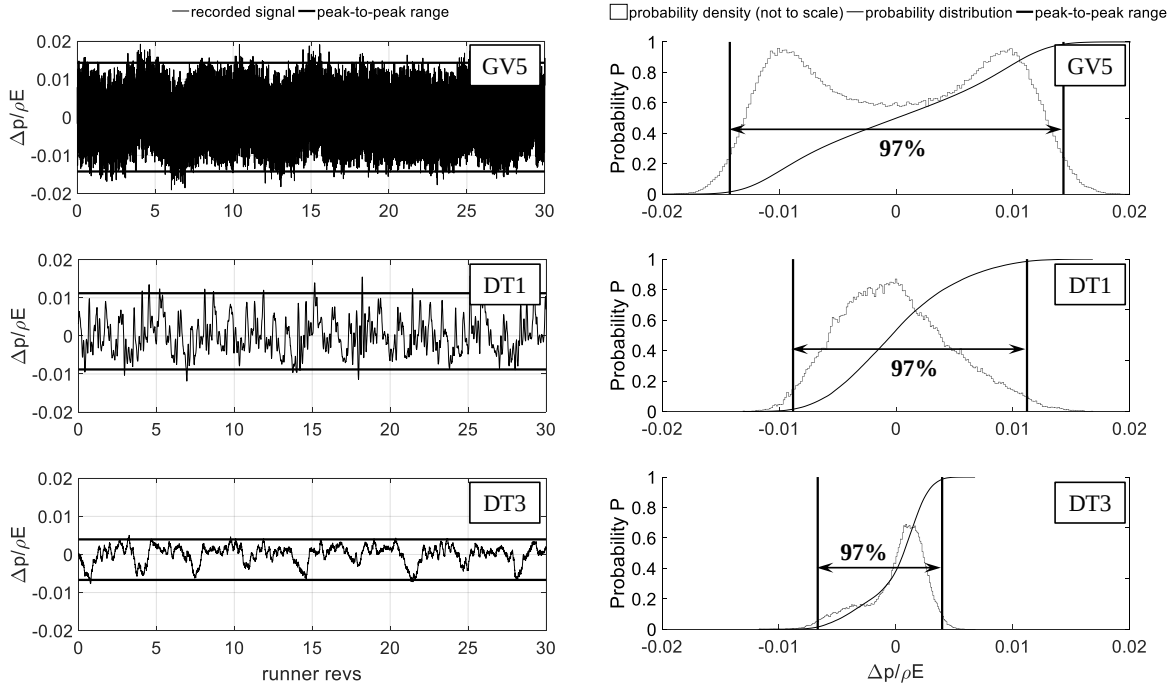

Figure 4. Example of the calculation of the peak-to-peak values using the Histogram method for the F99 runner operated at guide vane opening of $\alpha_{GV} = 6\ [deg]$ and speed factor of $n_{ED} = 0.18\ [-]$. On the left side, normalized time-domain signals for sensors marked with GV5, DT1 and DT3 respectively. On the right side, histogram representation showing the peak-to-peak range by retaining 97% in the middle for sensors marked with GV5, DT1 and DT3 respectively.

4. Results and discussion

The peak-to-peak values measured at the GV5 location are mainly due to the rotor-stator interaction (RSI), having the highest amplitude for the fundamental blade-passing frequency of $f \cdot Z_1$, where f is the rotational frequency of the runner in $[rps]$ and Z_1 is the number of runner blades at the inlet of the runner. This unsteady condition is driven by the two-way interaction between the periodic potential pressure fields existing in the channels of the guide vanes and the runner blades at different operating regimes. Figure 5 gives an example of a spectral analysis for the GV5 signal at the same operating point as shown on figure 4 above. The highest peak is at the frequency coefficient of $f_n = 30$ representing the fundamental blade passing frequency due to the 15 full length + 15 splitter blades of the F99 runner. Also visible but with considerably weaker amplitudes are the second harmonic at $f_n = 60$, the Rheingans frequency from the draft tube (explained below) and the half of the fundamental frequency at $f_n = 15$. This $1/2 \times f_{RSI}$ frequency comes from the slight variation of the pressure fields in the runner channels due to the design of the splitter blades.

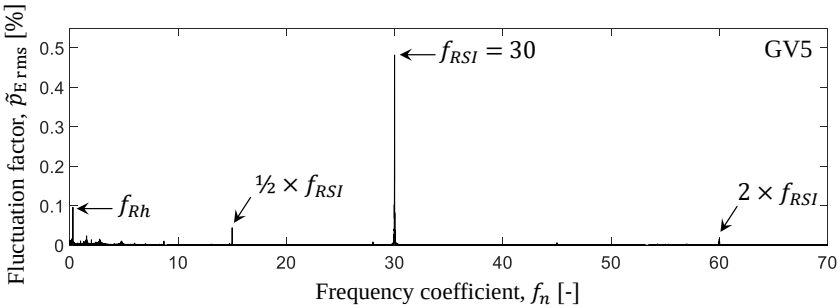

Figure 5. Spectral analysis of the time series from the sensor GV5 for the F99 runner operated at $\alpha_{GV} = 6\ [deg]$ and $n_{ED} = 0.18\ [-]$.

The pressure pulsations measured at the DT1 and DT3 sensors are dependent on the shape of the draft tube, the location of the sensors and the swirl number (a ratio between the swirl momentum and the axial momentum) calculated at the cross section where the sensors are located. Figure 6 summarizes the spectral results of the draft tube sensors for the operating point illustrated on figure 4, where the highest amplitude is for the first harmonic of the Rheingans frequency found at $f_{Rh} = 0.287$. These characteristic pressure pulsations are produced by the formation and movement of the corkscrew-like vortex that is rotating about the turbine axis. Due to the interaction of the aforementioned vortex with the draft tube elbow, a plunging plane wave is being created with the same Rheingans frequency of the vortex precession and a phase shift dependent on the measuring location in the draft tube cone. The decomposition of the signal to its synchronous (plunging pulsation) and asynchronous (rotating) component is done with a minimum of two sensors displaced by 180^0 in each measuring plane (here, sensors DT2 and DT4). Adding and subtracting the signals from the two sensors in each plane, and then dividing by two, will result in the synchronous and asynchronous components respectively. Moreover, the spectral analysis of both resulting components can provide an even deeper insights of the phenomenon. From the spectral results of the DT1 sensor on figure 6, additional peaks of synchronous and asynchronous nature can be spotted that are not harmonics of the Rheingans frequency and are not visible in the DT3 sensor. One reason could be that DT1 sensor is located very close to the runner outlet, capturing flow phenomenon existing in the runner channels that are diffused and weakened at the DT3 location. On the other hand, the spectral analysis of the DT3 sensor is clearly showing the Rheingans frequency and its higher harmonics, also visible to some extent in the synchronous and asynchronous components of the signal.

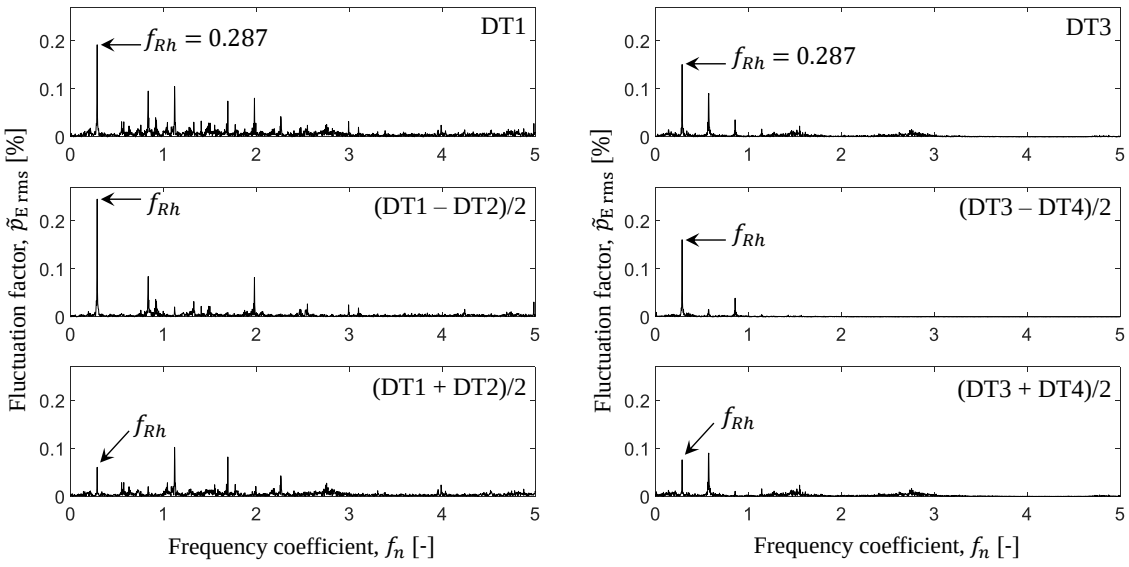

Figure 6. Spectral analysis of the time series, asynchronous and synchronous components from the draft tube sensors for the F99 runner operated at $\alpha_{GV} = 6\ [deg]$ and $n_{ED} = 0.18\ [-]$.

Results for the global performance of both runners are showed on figure 7, where due to simplification of the figures, labels of efficiency contours are omitted. The general appearance of the hill charts reveals the unique characteristics of each runner, as well as, the importance of the design aspects for operation at off-design operating conditions.

For the further discussion here, four operating regimes are defined and analyzed with respect to efficiency and pressure pulsations. If the turbines were installed and operated in an actual power plant, depending on the specifications of the waterways, net head will have slight variations at different turbine discharges. Hence, fixed (synchronous) speed operation of the turbine will result in operation along *nearly* vertical curves in the hill chart, with fixed position defined by the available net head. For the purpose of clarity and simplicity of the analysis in this paper, synchronous speed operation is assumed

to be happening along straight vertical lines instead, i.e. assuming constant net head in the entire range of the turbine discharges. Low specific-speed turbines and pump-turbines, such as the turbines investigated in the paper, are usually installed in high-head power plants, where due to reservoir constraints and technical reasons, head variation is within the range of $\pm 10\%$ of the rated head. Consequently, fixed speed operation is analyzed for three different scenarios, namely operation at optimal (design) head of the turbine and $\pm 10\%$ of that head (see hill chart legend on figure 7) serving as the extremes of the assumed head variation range. Same analysis can be done for other scenarios as well, but for the purpose of simplicity the paper deals with these three specific fixed-speed scenarios only.

On the other hand, variable-speed operation gives the opportunity to adjust and optimize the rotational speed of the runner according to the available head for each guide vane opening. This optimization can be done with respect to the maximization or minimization of any operational parameter of the turbine. In this paper, speed was optimized to give the highest possible efficiency for any operating condition, resulting in the red curves presented in the hill charts for both turbines on figure 7 below. For any power output of the turbine, according to the available net head, speed and guide vane opening can be found and set to give an operating point that will lie on the variable-speed curve in the hill chart. In order to achieve the maximum efficiency, the needed range of speed variation is relatively larger for the RPT runner when compared with the F99, which can be seen from the n_{ED} range that is covered by the variable-speed operation curve.

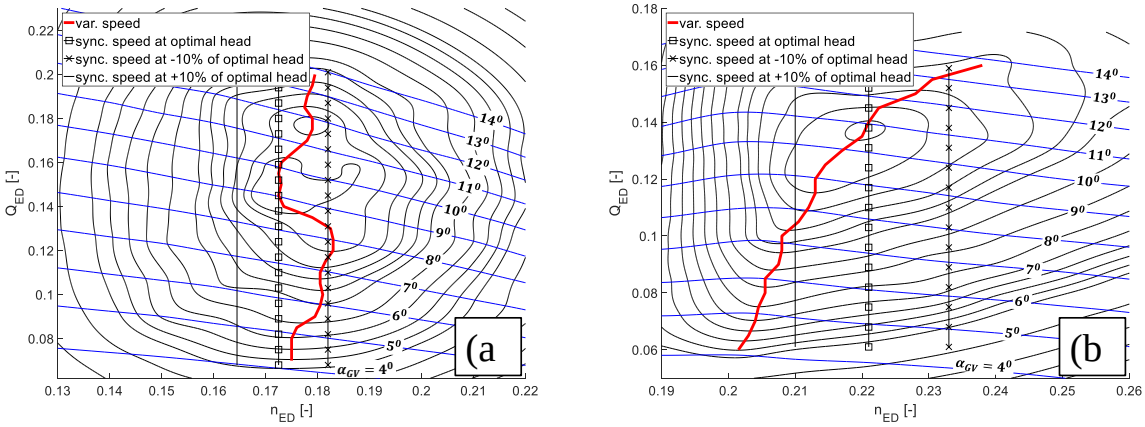

Figure 7. Hill charts of efficiency for both runners. a) the F99 runner and b) the RPT runner.

Due to the specific hydraulic design of the F99 runner, when comparing the efficiency between variable and synchronous speed operation (see figure 8a), up to 1.2% increase of the absolute hydraulic efficiency can be only expected if the head variation is $\pm 10\%$ of the optimal head or larger. For the case when the head variation is relatively small and close to the optimal head, variable-speed operation of the F99 will never give more than 0.5% increase of the absolute hydraulic efficiency. When it comes to the pressure pulsations, however, operation along the optimized variable-speed curve gives promising results for the F99 runner, especially in the vaneless space (see figures 8b, 8c and 8d). As it can be seen from figure 8b, when operated at variable-speed the peak-to-peak values are either reduced or kept in the same level as for synchronous-speed operation at optimal head for the entire range. Synchronous-speed operation at head 10% lower than the optimal head gave the lowest pressure pulsations in the vaneless space, indicating that, with some efficiency reduction, the speed variation can be optimized to give the lowest possible pressure fluctuations in the vaneless space, or any other particular location. In the draft tube cone of the F99 runner (see figures 8c and 8d), variable-speed operation at partial load gave slightly higher pressure fluctuations when compared to the synchronous-speed operation at the optimal head. For the case when the head is 10% higher than the optimal, the absolute efficiency at synchronous-speed operation is more than 1% lower compared to the variable-speed operation, but the pressure fluctuations in the draft tube are always higher for the variable-speed operation. This indicates that the hydraulic efficiency and the pressure fluctuations in the F99 runner are not directly correlated.

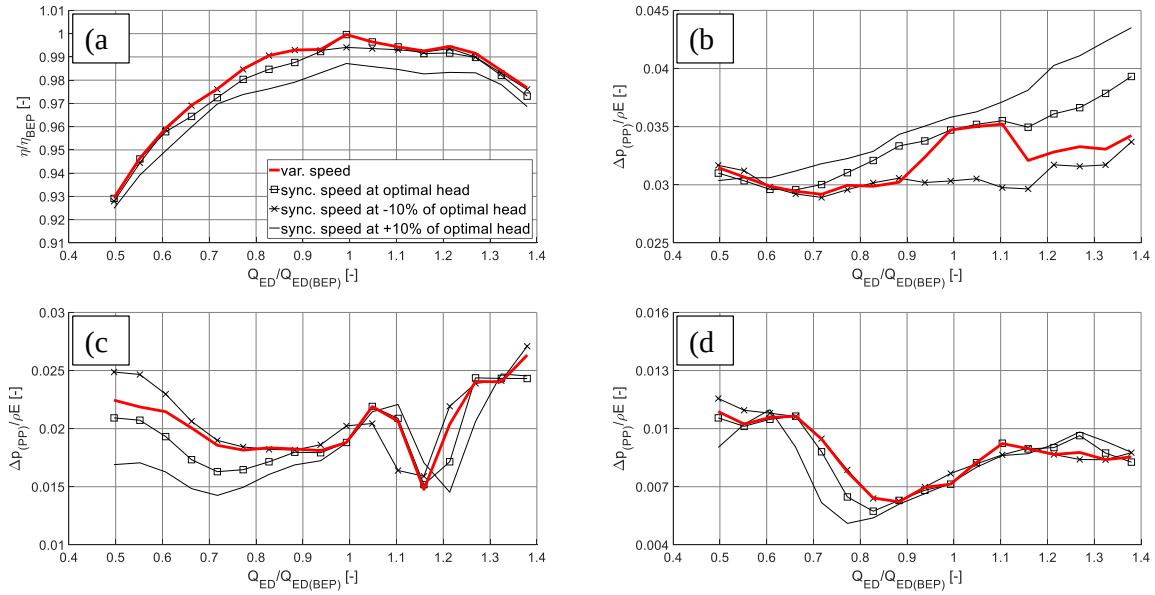

Figure 8. Comparison of measured efficiency and pressure pulsations between variable-speed and synchronous speed operation of the F99 runner. a) normalized hydraulic efficiency, b) normalized peak-to-peak values at the GV5 location, c) normalized peak-to-peak values at the DT1 location and d) normalized peak-to-peak values at the DT3 location. Same legend applies for (b, (c and (d.

Analyzing the results of the RPT runner, having a totally different hydraulic design compared to the F99 runner [19], the absolute efficiency increase for variable-speed operation can be up to 1% compared to the synchronous-speed operation at the optimal head, or up to 2.2% for head 10% lower than the optimal (see figure 9a). Due to the lower number of runner blades for the RPT runner, giving relatively higher blade loading, normalized pressure fluctuations in the vaneless space are much higher when compared to the F99 runner.

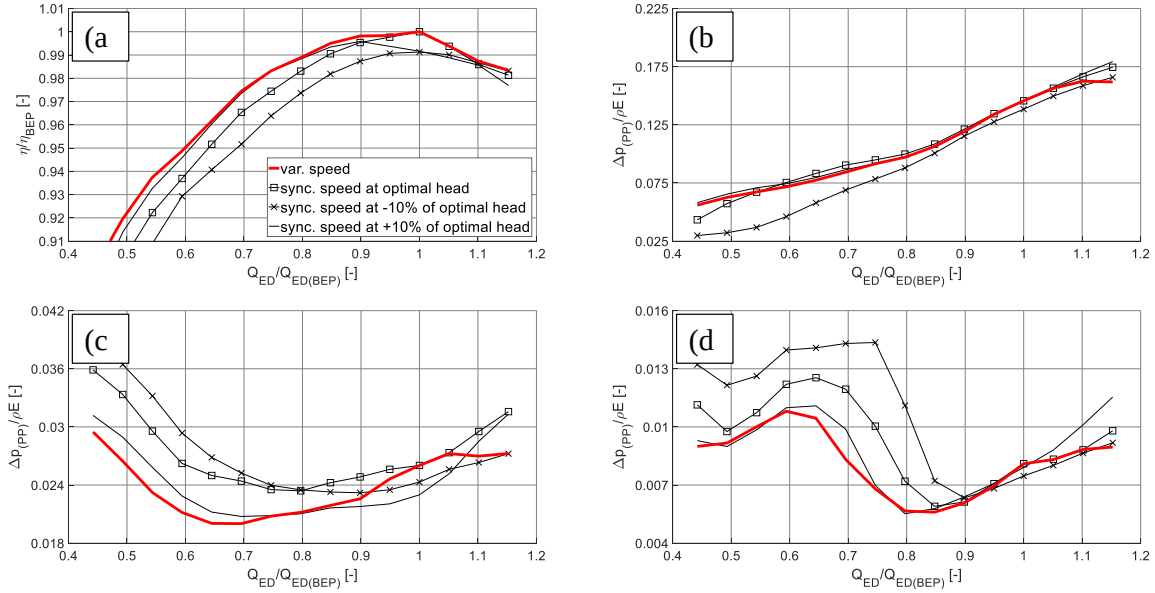

Figure 9. Comparison of measured efficiency and pressure pulsations between variable-speed and synchronous speed operation of the RPT runner. a) normalized hydraulic efficiency, b) normalized peak-to-peak values at the GV5 location, c) normalized peak-to-peak values at the DT1 location and d) normalized peak-to-peak values at the DT3 location. Same legend applies for (b, (c and (d.

Optimized speed operation made relatively small changes for the pressure fluctuations at the GV5 location (see figure 9b), and the peak-to-peak values stayed at the same level as for the synchronous-speed operation at optimal head. For the pressure fluctuations in the draft tube cone, variable-speed operation gave significant reduction of the peak-to-peak values, having the lowest pulsations at partial loads for the entire range compared to any scenario of the synchronous-speed operation (see figures 9c and 9d). Similarly as found for the F99 runner, the hydraulic efficiency and the pressure fluctuations in the RPT runner are not directly correlated. To illustrate this, pressure fluctuation iso-contours of the normalized peak-to-peak values from the GV5 sensor for both runners are shown on figure 10. The efficiency optimized variable-speed path (red line) is clearly far from the zone where pressure fluctuations are lowest in the vaneless space. Similar behavior was observed for all sensors mounted in the turbines.

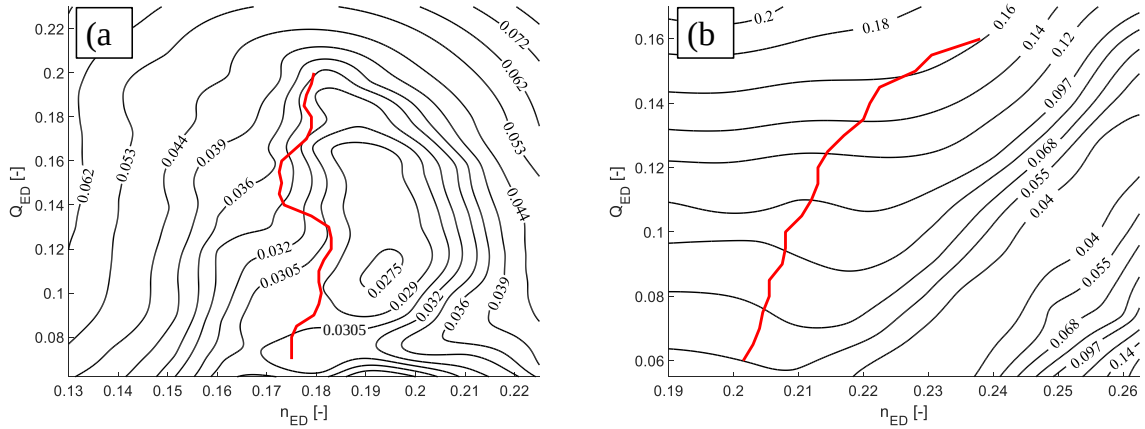

Figure 10. Location of the variable-speed operation curves on top of the normalized peak-to-peak contours for the GV5 sensor. a) the F99 runner and b) the RPT runner.

5. Conclusions

Synchronous-speed operation away from the design point reduces the efficiency and affects the pressure fluctuations in the turbine. Variable-speed operation gives additional flexibility since the rotational speed of the runner can be optimized and adjusted to improve either efficiency or the pressure pulsations in the full operating range of the turbine. In this paper, laboratory measurements were conducted for one low-specific-speed Francis turbine runner and one low-specific-speed pump-turbine runner that were designed to fit in the same rig, using a common distributor and draft tube. The overall hydraulic efficiency and the pressure pulsations in the vaneless space and the draft tube were measured for a wide operating range comprising of more than 200 operating points for each turbine runner. Histogram method was used to quantify the peak-to-peak values of the fluctuating pressure, mapping the entire operational range similarly as for the hydraulic efficiency. Rotational speed of both runners was optimized to give the maximum efficiency for each discharge factor Q_{ED}.

Due to the different hydraulic design that both runners have, different gain in efficiency and pressure pulsation intensities was achieved from variable-speed operation. Synchronous-speed operation was assessed for three scenarios assuming constant net head in the entire range of the discharge, namely, (1) operation at optimal head, (2) operation at +10% of the optimal head, and (3) operation at -10% of the optimal head. Efficiency and pressure pulsations at optimized rotational speeds were compared against the three synchronous-speed operation scenarios for both turbine runners. Variable-speed operation of the splitter-bladed Francis runner (F99) gave maximum hydraulic efficiency gain of 0.5% when compared to the synchronous-speed operation at optimal head. Up to 1.2% hydraulic efficiency gain was achieved when comparing against the synchronous-speed operation at +10% of the optimal head. Pressure pulsations in the vaneless space were reduced when operated at variable-speed, with none-to-slight increase of the pressure pulsations observed in the draft tube cone.

For the reversible pump-turbine (RPT), variable-speed operation gave slightly higher efficiency gain, resulting in up to 1% for the entire range when compared to the synchronous-speed operation at

the optimal head and up to 2.2% for the comparison at head 10% lower than the optimal head. Variable-speed operation gave insignificant changes of the pressure pulsations in the vaneless space, but gave the lowest pressure pulsations in the draft tube at partial loads for the entire operating range. No direct connection between hydraulic efficiency and peak-to-peak values was observed, indicating that speed optimization can be done with respect to only one performance parameter of the turbine, or as a tradeoff between several.

References

[1] Dörfler P, Sick M and Coutu A 2013 Flow-induced pulsation and vibration in hydroelectric machinery *Springer-Verlag* London p 244 (DOI: 10.1007/978-1-4471-4252-2)
[2] Trivedi C and Cervantes M J 2017 Fluid-structure interactions in Francis turbines: A perspective review *Renewable and Sustainable Energy Reviews* **68** 87-101
[3] Tanaka H 2011 Vibration behavior and dynamic stress of runners of very high head reversible pump-turbines *Int. Journal of Fluid Machinery and Systems* **4** 289-306
[4] Seidel U, Mende C, Hubner B, Weber W and Otto A 2014 Dynamic loads in Francis runners and their impact on fatigue life *27th IAHR Symposium on Hydraulic Machinery and Systems, IOP Conf. Series: Earth and Environmental Science* **22** 032054
[5] Gagnon M, Tahan S A, Bocher P and Thibault D 2010 Impact of Startup Scheme on Francis Runner Life Expectancy *25th IAHR Symposium on Hydraulic Machinery and Systems, IOP Conf. Series: Earth and Environmental Science* **12** 012107
[6] Minakov A V, Platonov D V, Dekterev A A, Sentyabov A V and Zakharov A V 2015 The analysis of unsteady flow structure and low frequency pressure pulsations in the high-head Francis turbines *International Journal of Heat and Fluid flow* **53** 183-194
[7] Raabe J 1985 Hydro power - the design, use, and function of hydromechanical, hydraulic, and electrical equipment *VDI Verlag, Düsseldorf* p 684
[8] Farell C and Gulliver J 1987 Hydromechanics of variable speed turbines *Journal of Energy Engineering* **113(1)** 1-13
[9] Heckelsmueller G P 2015 Application of variable speed operation on Francis turbines *Ingenieria e Investigacion* **35(1)** 12-16
[10] Fraile-Ardanuy J, Wilhelmi J R, Fraile-Mora J J and Perez J I 2006 Variable-speed hydro generation: Operational aspects and control *IEEE Trans. on Energy Conv.* **21(2)** 569-574
[11] Perez J I, Wilhelmi J R and Maroto L 2008 Adjustable speed operation of a hydropower plant associated to an irrigation reservoir *Energy Conversion and Management* **49** 2973-2978
[12] Hell J 2017 High flexible hydropower generation concepts for future grids *J. Phys.: Conf. Ser.* **813** 012007
[13] Schafer D and Simond J J 1998 Adjustable speed asynchronous machine in hydro power plants and its advantages for the electric grid stability *CIGRE report* 1-8
[14] Claude J M 2017 Performances achieved to the grid by a full power converter used in a variable speed pumped storage plant *J. Phys.: Conf. Ser.* **813** 012008
[15] IEC-60193 1999 Hydraulic Turbines, Storage Pumps and Pump-turbines: Model Acceptance Tests *International standard, International Electro-Technical Commission* **3(1)** 1-578
[16] Ciocan G D, Iliescu M S, Vu T C, Nennemann B and Avellan F 2007 Experimental study and numerical simulation of the FLINDT draft tube rotating vortex *Journal of Fluids Engineering* **129(2)** 146-158
[17] Trivedi C, Cervantes M and Dahlhaug O G 2016 Experimental and Numerical studies of a High-Head Francis Turbine. A review of the Francis-99 Test Case *Energies* **9(2)** 1-24
[18] Olimstad G, Borresen B and Nielsen T K 2011 Stability limits of reversible-pump turbines in turbine mode of operation and measurements of unstable characteristics *Journal of Fluids Engineering* **134(11)** 121102
[19] Iliev I, Trivedi C and Dahlhaug O G 2018 Simplified hydrodynamic analysis on the general shape of the hill charts of Francis turbines using shroud-streamline modelling *J. Phys.: Conf. Ser.* **1042** 012003